

Supporting information

Structural and dynamical insights into SilE silver binding from combined analytical probes

Yoan Monneau^a, Cyrielle Arrault^a, Coraline Duroux^a, Marie Martin^a, Fabien Chirot^b, Luke Mac Aleese^b, Marion Girod^a, Clothilde Comby-Zerbino^b, Agnès Hagège^a, Olivier Walker^a and Maggy Hologne^a

^a Université de Lyon, CNRS, UCB Lyon1, Institut des Sciences Analytiques, UMR5280, 5 rue de la Doua, Villeurbanne 69100, France

^b Univ Lyon 1, Université Claude Bernard Lyon 1, CNRS, Institut Lumière Matière, UMR5306, Cité Lyonnaise de l'Environnement et de l'Analyse, 5 rue de la Doua, Villeurbanne 69100, France

Protein expression and purification

The SilE²¹⁻¹⁴³ and SilE⁵⁷⁻⁹⁵ constructs in pEtM-60 (Novagen) were expressed with N terminus fused to NusA and a hexa histidine tag (His6 tag). The constructs were transformed into *E. coli* BL21 Gold (DE3) for overexpression. Cells were grown either in LB medium with 50 mg/L kanamycin or uniform isotopic labeling in M9 medium supplemented with 1 mM MgSO₄, 1 mM CaCl₂, 4 g/L D-glucose, 6 mg/L thiamine, 50 mg/L kanamycin, 1 % (vol/vol) trace element solution [5 g/L EDTA, 0.5 g/L FeCl₃, 6H₂O, 5 mg/L ZnO, 1 mg/L CuCl₂, 2H₂O, 1 mg/L Co (NO₃)₂, 6H₂O and 1 mg/L (NH₄)₆Mo₇O₂₄, 4H₂O] and 1 g/L ¹⁵NH₄Cl as main nitrogen source. For ¹³C-labeled protein ¹²C₆-D-glucose was exchanged for 2.5 g/L ¹³C₆-D-glucose. The cells were grown at 37°C until OD600 reached 0.6-0.8 and were induced by the addition of 1 mM IPTG. Induction was performed for 4h at 37°C. The cells were lysed in 50 mM Tris-base, 300 mM NaCl, 5 mM imidazole, 5 % (vol/vol) glycerol and pH 7.8-8. The clarified cell lysate was loaded on Ni-NTA Superflow column (Qiagen) equilibrated with 50 mM Tris-base, 300 mM NaCl, 5 mM imidazole, 10 % (vol/vol) glycerol, and pH 7.8-8. The bound protein was eluted by applying an imidazole gradient. NusA and His6 tags were removed by cleavage with tobacco etch virus (TEV) protease at 5°C overnight. After dialysis against lysis with 50 mM Tris-base, 150 mM NaCl, 5 mM b-Me, and pH 7.8-8. SilE constructs are separated from NusA-His6 by second Ni²⁺ affinity chromatography using as a first step elution with 10% of solution (50 mM Tris-base, 300 mM NaCl, 500 mM imidazole, 10 % (vol/vol) glycerol and pH 7.8-8) and then a gradient elution. To obtain an improved purity, we performed size-exclusion chromatography using a Superdex 75 16/60 column (GE Healthcare) in 20mM NaF, 20 mM MES and pH 6.8.

NMR experiments

NMR experiments were carried out at 283K with a spectrometer Bruker Avance III HD operated at a ¹H frequency of 600 MHz (14.1 T) and equipped with a triple HCN probe. All the NMR samples were prepared at a concentration of 140 μM in 20 mM MES buffer (pH 6.8) complemented by 20 mM NaF and 10 % D₂O. The backbone resonance assignments of SilE have been performed using a combination of the classical 3D experiments: HNCA, HNCOCA, HNCACB, and CBCACONH.

The interaction studies have been carried out using chemical shift perturbation (CSP) measurement, where a series of ¹H-¹⁵N HSQC were recorded for a protein while adding a small volume of the concentrated silver solution (AgNO₃). A calibration curve for different known concentration of silver ions has been carried out by measuring the potential of the solutions using a silver specific electrode. Thus, the accuracy of the silver

solution concentration has been checked before any experiments. The combined CSP is calculated using the following equation:

$$\Delta\delta = \sqrt{(\Delta\delta_H)^2 + \left(\frac{\Delta\delta_N}{5}\right)^2}$$

Relaxation experiments including ^{15}N longitudinal (R_1) and transversal (R_2) relaxation as well as the ^1H - ^{15}N heteronuclear cross-relaxation rates were recorded. For the R_1 experiments, we used relaxation delays ranging from 40 to 2000 ms with a recycling delay of 3.5 s. In the case of the R_2 experiments, we used relaxation delays ranging from 8 to 480 ms with a recycling delay of 3.5 s. For ^1H - ^{15}N heteronuclear NOE experiments, 2D spectra were recorded with and without presaturation of amide protons. The relaxation delay was set to 4.5 s to allow the bulk water magnetization to return as close as possible to the equilibrium state.

CE-ICP-MS experiments

Separations were carried out on an AB Sciex instrument using the 32 Karat Software, using a fused silica capillary (75 μm x 45 cm) thermally coated using hydroxypropyl cellulose. An Agilent 7700 ICP/MS equipped with a Micromist micro nebulizer was used for the specific detection of silver. The hyphenation between CE and ICP/MS was achieved via a homemade sheath-flow interface described elsewhere.¹

Samples were hydrodynamically injected (0.5 psi for 5 s) and separations were performed under -15 kV + 0.5 psi at 25°C with MES 20 mM, NaF 20 mM, pH 6.8 electrolyte and followed by a pressure step with 1 mM HNO_3 , to release Ag^+ sorbed onto the capillary walls. The signal at m/z 107 was monitored using an integration time of 1 s. ICP operating conditions were the following: nebulizer gas flow rate: 1 L/min, plasma gas flow rate: 15 L/min, auxiliary gas flow: 0.9 L/min, and radiofrequency power 1550 W. Between runs, the capillary was washed with the BGE for 3 min under 5 psi.

HR-MS experiments

Experiments were performed on a hybrid quadrupole-orbitrap QExactive® mass spectrometer (Thermo Fisher Scientific, San Jose, CA, USA) equipped with a HESI ion source. For MS analysis of intact proteins, 5 μM of SilE solutions in presence of 1 to 10 molar equivalents of silver ions in MES were injected by Flow Injection Analysis in $\text{H}_2\text{O}/\text{ACN}$ 1:1 (% v:v) solvent at a 3 $\mu\text{L}/\text{min}$ flow rate using a Thermo Scientific Dionex UltiMate 3000 pump and autosampler system. Electrospray ionization in the HESI source was achieved in positive ion mode with a spray voltage of 4 kV at 320°C, and sheath gas and auxiliary gas flow rates were 12 and 4 (arbitrary unit), respectively. The Automatic Gain Control (AGC) target was set to $1\text{e}6$, paired with a maximum injection time of 100 ms. The S-Lens RF level was set to 55 (arb. unit). Resolution in the orbitrap analyzer was set to 140,000 for full MS spectra.

For proteomic MS/MS analysis, protein samples (200 μg of SilE and 200 μg of SilE + 6 equivalents of Ag^+) were denatured in 8 M urea at 60°C for 40 min. To reduce the urea concentration, the samples were diluted 5-fold with AMBIC before overnight digestion at 37°C with trypsin using a 1:30 (w/w) enzyme to substrate ratio. Digestion was stopped by the addition of formic acid to a final concentration of 0.5%.

All samples were desalted and concentrated using Oasis™ HLB 3cc (60 mg) reversed-phase cartridges (Waters, Milford, MA, USA). Before loading the tryptic digest onto the Oasis cartridges, all cartridges were conditioned with 1 mL of MeOH and then 1 mL of water containing 0.5% FA. After the loading, all cartridges were washed with 1 mL of

MeOH/water (5/95, v/v) containing 0.5 % FA and eluted with 1.5 mL of MeOH containing 0.5 % FA. All samples were evaporated to dryness and resuspended in 100 μ L of water/ACN (95:5, v/v) containing 0.5% FA.

The HPLC separation was carried out on an XBridge C18 column (100 X 2.1 mm, 3.5 μ m) from Waters. The HPLC mobile phase consisted of water containing formic acid 0.1 % (v/v) as eluent A, and ACN containing formic acid 0.1% (v/v) as eluent B. Elution was performed at a flow rate of 300 μ L/min. The elution sequence, for the digested protein samples, included a linear gradient from 5 % to 45 % of eluent B for 52 min, then a plateau at 95 % of eluent B for 4 min. The gradient was returned to the initial conditions and held there for 4 min. The injection volume was 10 μ L.

Ionization was achieved using electrospray in the positive ionization mode with an ion spray voltage of 4 kV. The sheath gas and the auxiliary gas (nitrogen) flow rates were respectively set at 35 and 10 (arbitrary unit) with a HESI vaporizer temperature of 400°C. The ion transfer capillary temperature was 300°C with a sweep gas (nitrogen) flow rate at 5 (arbitrary unit). The S-lens RF was set at 90 (arbitrary unit). The AGC target was 3e6 and the maximum injection time was set at 250 ms. Experiments were done in data-dependent top 10 mode. The full MS scans were done over an m/z 300-1500 range with a resolution of 35 000. For the data-dependent MS/MS scans, the resolution was set at 17 500, isolation 2 m/z , with a normalized collision energy of 28 (arbitrary unit). To exclude the redundant processing of dominant ions and allow selection of low abundant oxidized peptides, a dynamic exclusion time of 20 s was set. Fragmentation spectra were converted to .mgf format using MSConvert and searched against fasta of *Salmonella typhimurium* proteins and decoys using SearchGui.² All searches used the following parameters: mass tolerances in MS and MS/MS modes were 10 ppm and 20 ppm, respectively. Trypsin was designated as the enzyme and up to two missed cleavages were allowed. The considered standard variable modifications were asparagine deamidation and methionine oxidation. Results were visualized using ProlineStudio 2.1³ and validated by ensuring FDR (false discovery score) \leq 1% on scores.

IM-MS experiments

IM-MS experiments were performed on homemade dual drift tube instruments coupled upstream with a Maxis Impact Quadrupole-Time-of-Flight mass spectrometer (Bruker, Bremen, Germany). The instrument is described in detail in ref ⁴. The IM-MS cell is filled with helium at 4 Torr and contains two 79 cm-long drift tubes in series across which a constant axial electric field of 200 to 750 V.m⁻¹ is applied. Both tubes can be used as a single high-resolution drift cell. In addition, an ion gate at the end of the first drift tube allows the selection of ions as a function of their drift time. Selected ions can then be accelerated in the drift gas to trigger collisional activation. The products are finally analyzed in the second drift tube. In both modes, IM-MS arrival time distributions (ATDs) were extracted for ions of selected m/z from mass spectra recorded as a function of arrival time.

The SiLE samples were first desalted using dialysis tubes (3,5 kDa, Roth). For electrospray, we used solutions at 20 μ mol.L⁻¹ of protein in ammonium acetate buffer at 50 mmol.L⁻¹. Silver nitrate was finally added in different concentrations just before the experiment. These solutions were sprayed directly using a custom nano-electrospray source based on homemade borosilicate emitter tips (5 μ m tip diameter) thermalized by a Peltier module at typically 17°C, to stabilize the ion signal. The glass capillary transfer was maintained to 27°C.

CD experiments

CD experiments were acquired at 25°C for SilE²¹⁻¹⁴³ and SilE⁵⁷⁻⁹⁵ constructs on a Chirascan spectrometer (Applied Photophysics). Protein concentration was set to 20 μM. Each sample was prepared in 20 mM MES buffer at pH 6.8 supplemented by 20 mM NaF. Ten repetitions have been recorded for each equivalent of Ag⁺ in solution.

SAXS experiments

SAXS measurements of [SilE:nAg] complex were performed at the ESRF BioSAXS beamline BM29 (Grenoble, France), using a 2D Pilatus detector at an X-ray wavelength $\lambda = 1.008 \text{ \AA}$ with a standard single instrumental configuration (samples being automatically mounted to a capillary and 10 frames with 1 s exposure using the flow-through mode) at 20 °C. Data processing and reduction were performed using an automated standard ESRF beamline software (BSxCuBE)⁵ and PRIMUS⁶ while the overall parameters derived from SAXS data were processed with SCATTER.⁷ Data were measured at different concentrations (1, 2, and 4 mg/ml) in HEPES buffer (20 mM, pH 7.8) to eliminate any inter-particle effects and merged where needed. It allows obtaining high-quality data from both the low angle range (low protein concentration to accurately extract the radii of gyration) and from the high angle range (high protein concentration for an accurate solvent subtraction).

AlphaFold and MultiFoXS N-state modeling

To model a putative silver-bound structure, we have used the ColabFold server,⁸ based on the AlphaFold 2 prediction protocol,⁹ and the sequence of SilE is given by the UniProt accession number Q9Z4N3.

The modeled structures have been ranked according to pLDDT and PAE. To estimate the quality of the predicted structures, AlphaFold produces a per-residue confidence metric called the predicted local distance difference test (pLDDT) on a scale from 0 to 100. The pLDDT metric estimates how well the prediction would agree with an experimental structure based on the local distance difference test C α (lDDT-C α).¹⁰ A pLDDT < 50 should not be interpreted except as a possible disorder prediction while a cut-off of pLDDT > 70 corresponds to a generally correct backbone prediction.¹¹ It is well-calibrated and full details on how the pLDDT is produced are given in the supplementary information of the AlphaFold paper.⁹ The second metric used to estimate the accuracy of AlphaFold modeling is based on the Predicted Aligned Error (PAE) that estimates the confidence about domain positioning. A consistently low PAE suggests AlphaFold is confident about the relative domain positions. Consistently high PAE suggests that the relative positions of the domains should not be interpreted.

We have retained the structure that obtained the highest pLDDT while the domain positioning has been modified by tuning the different levels of flexibility of SilE. Consequently, to characterize the range of conformations consistent with the SAXS data for the [SilE:nAg] complex, we have analyzed the distribution of R_g through MultiFoXS N-state modeling.¹² As an input, we have provided the PDB rank1 structure derived from AlphaFold prediction. SilE flexible regions have been defined according to Supplementary Table 2 and 10000 conformers have been sampled. In the first step, MultiFoXS samples the input structures with an RRT algorithm,¹² significantly improving the sampling efficiency compared to random sampling. As a second step, a SAXS profile is calculated for each sampled conformation. Finally, the 1000 top N-states models are sorted according to their χ score values.

Fig. S1 | **SiE sequence** (*Salmonella Typhimurium*) with respect to UniProt accession number Q9Z4N3. The different HxxM or MxxH motifs are displayed in blue.

```
      20          30          40          50          60
GAMG TETVNIHERV NNAQAPAHHQM QSAAAPVGIQ GTAPRMAGMD

      70          80          90          100
QHEQAIIAHE TMTNGSADAH QKMVESHQRM MGSQTVSPTG

      110         120         130         140
PSKSLAAMMNE HERAAVAHEF MNNGQSGPHQ AMAEAHRRML SAG
```

Fig. S2 | ESI-MS spectra observed for the 5 μ M solution of A) SiE and B) in presence of 5 equivalents of silver ions. The insert in B) shows a zoom on the m/z range of the 16^+ [SiE:nAg] complexes.

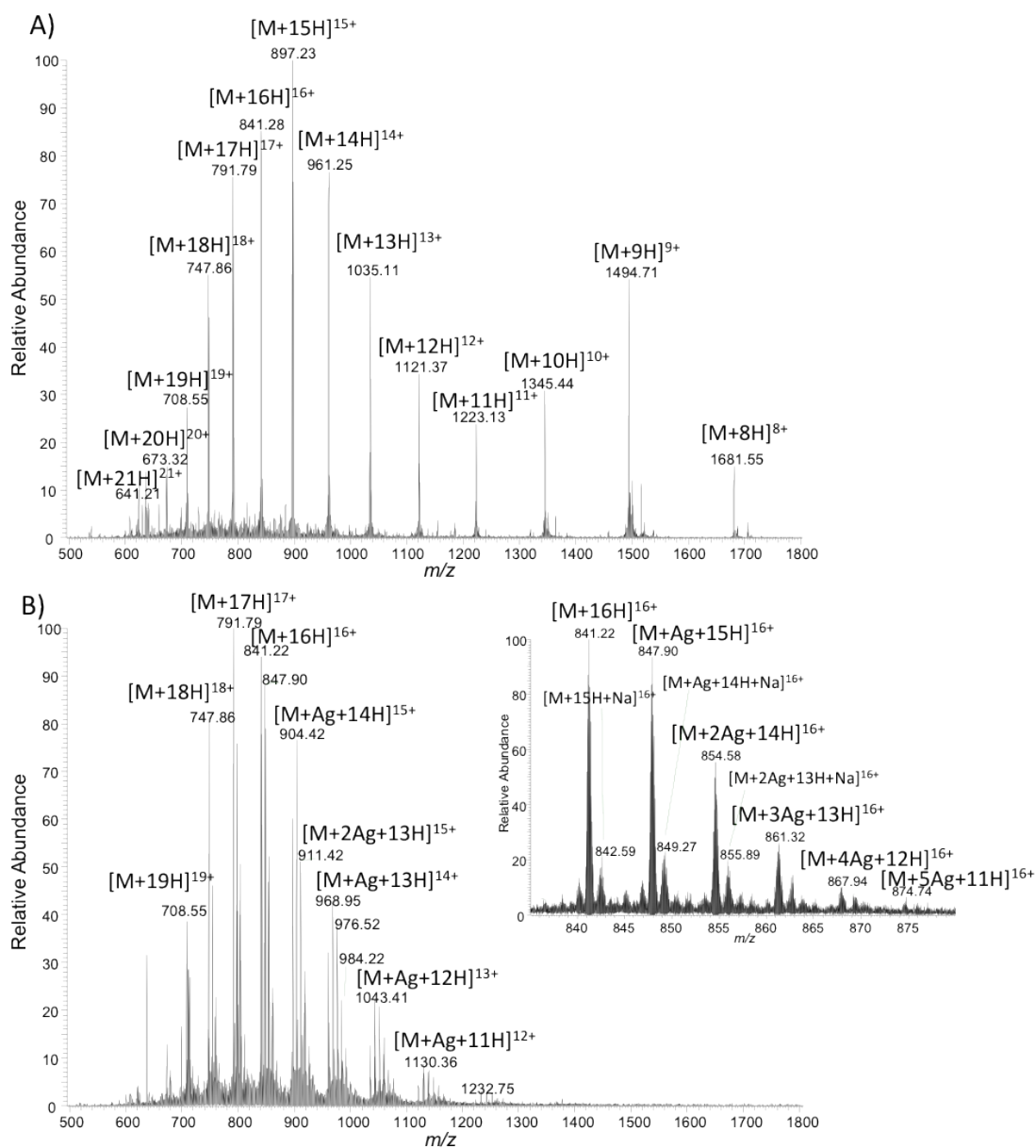


Fig. S3 | 2D ^1H - ^{15}N HSQC NMR spectra of SiIE in the free state and in the presence of 1 to 9 equivalents of silver solution.

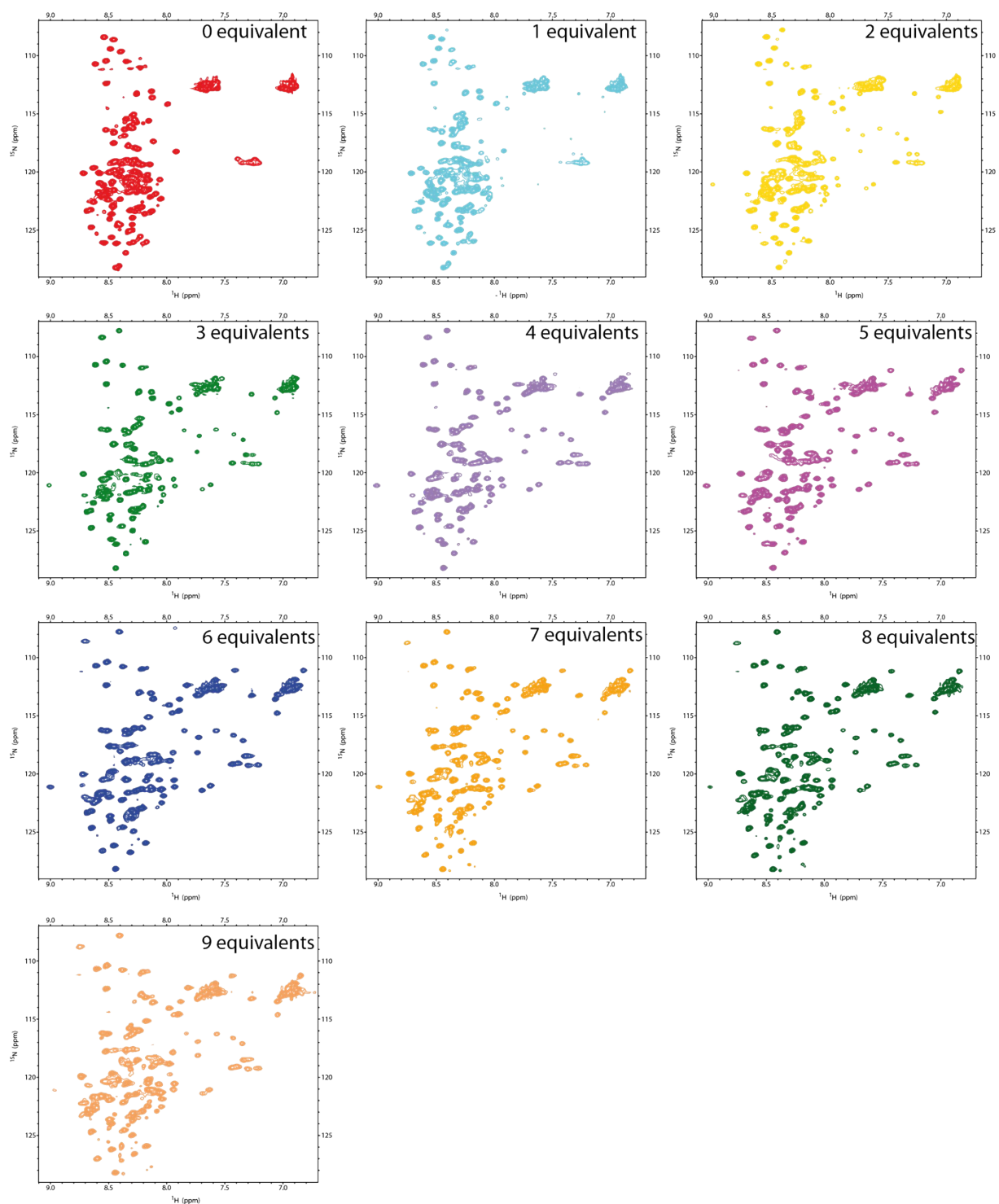
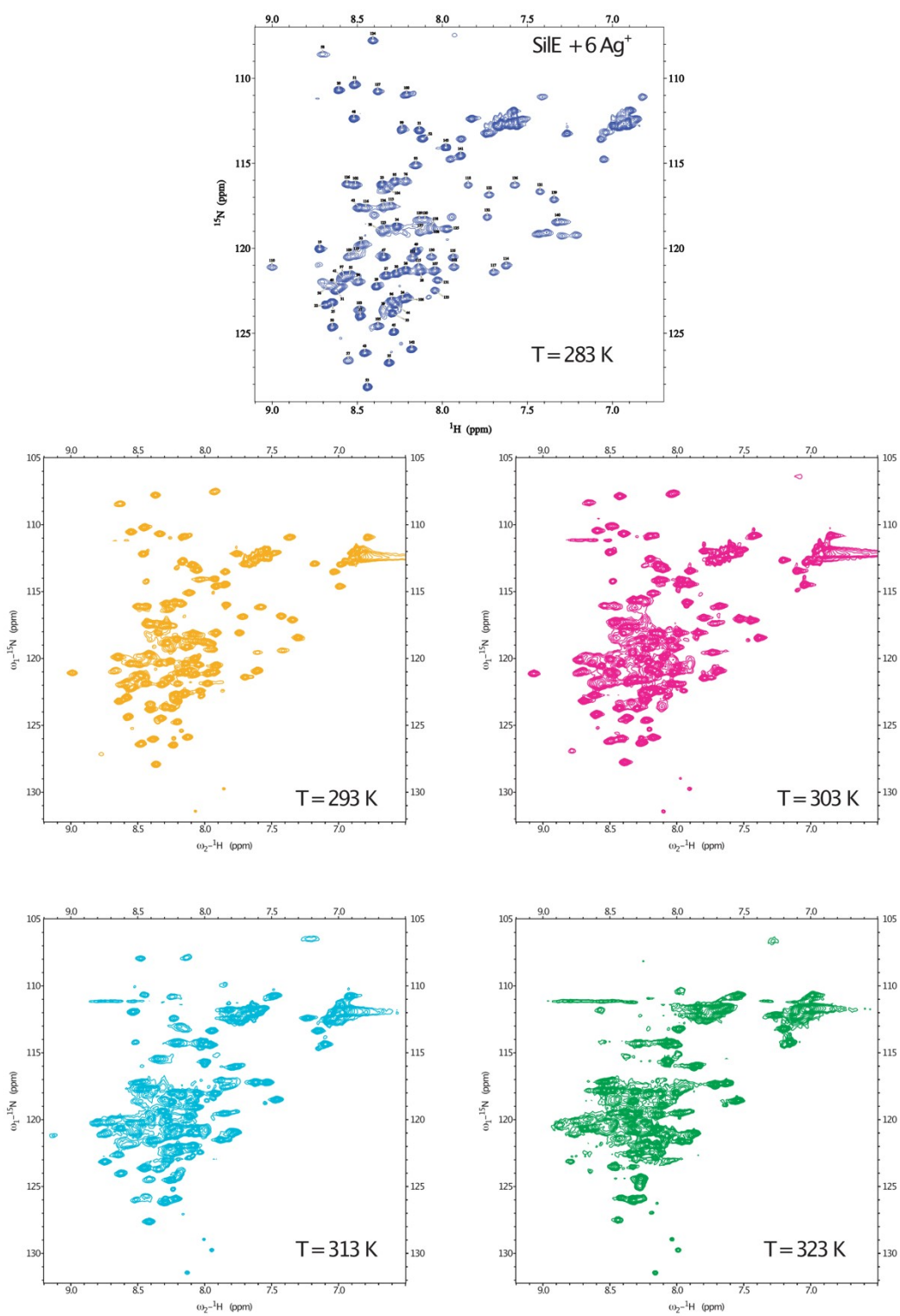
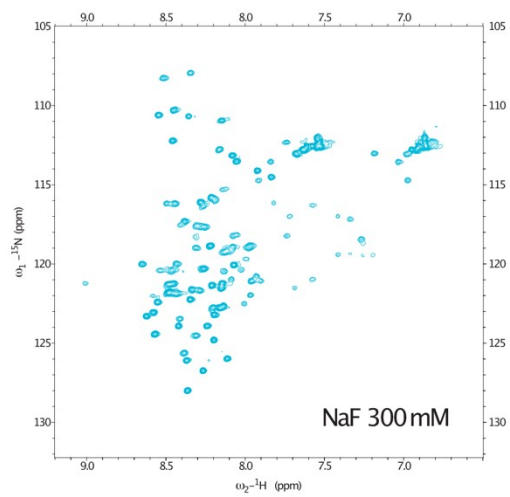
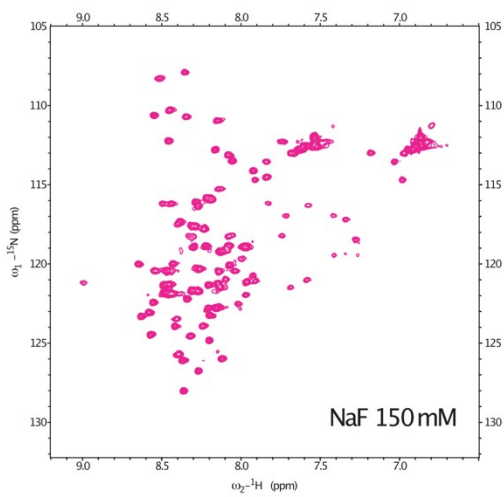
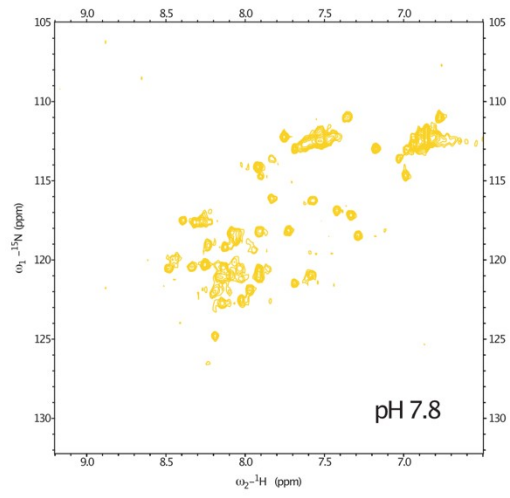
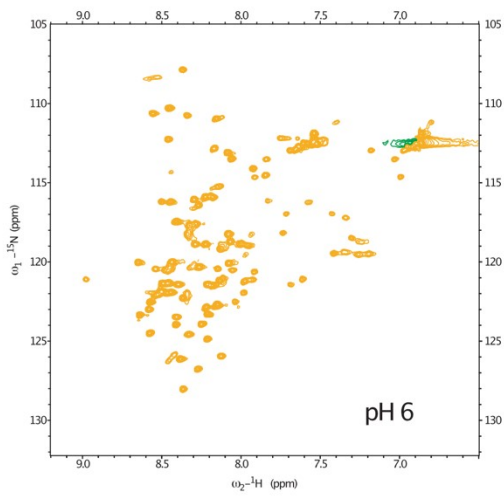
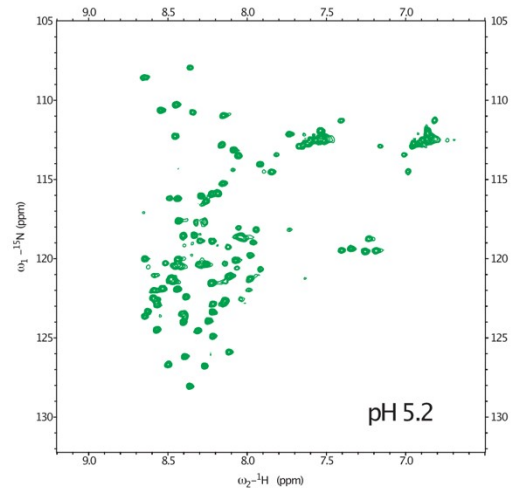
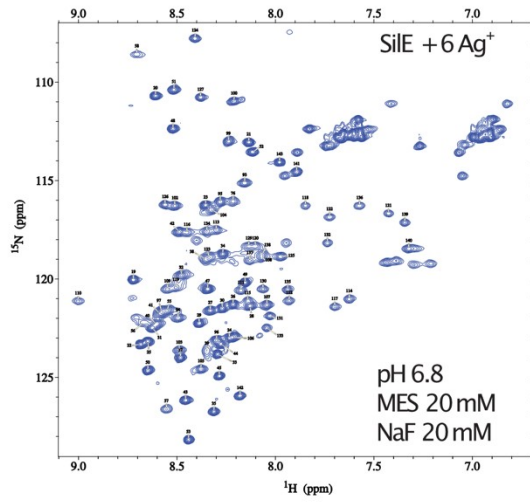


Fig. S4 | 2D ^1H - ^{15}N HSQC NMR spectra of SiIE in presence of 6 equivalents of silver ions for A) temperatures ranging from 283 to 323 K, B) different pH and ionic strength conditions, C) recorded at a ^1H frequency of 600 MHz (red) and 900 MHz (blue) where the * peaks correspond to refolded side chains protons and D) different pressures from 1 to 2250 bars at 293 K and from 1 to 2000 bars at 278 K.

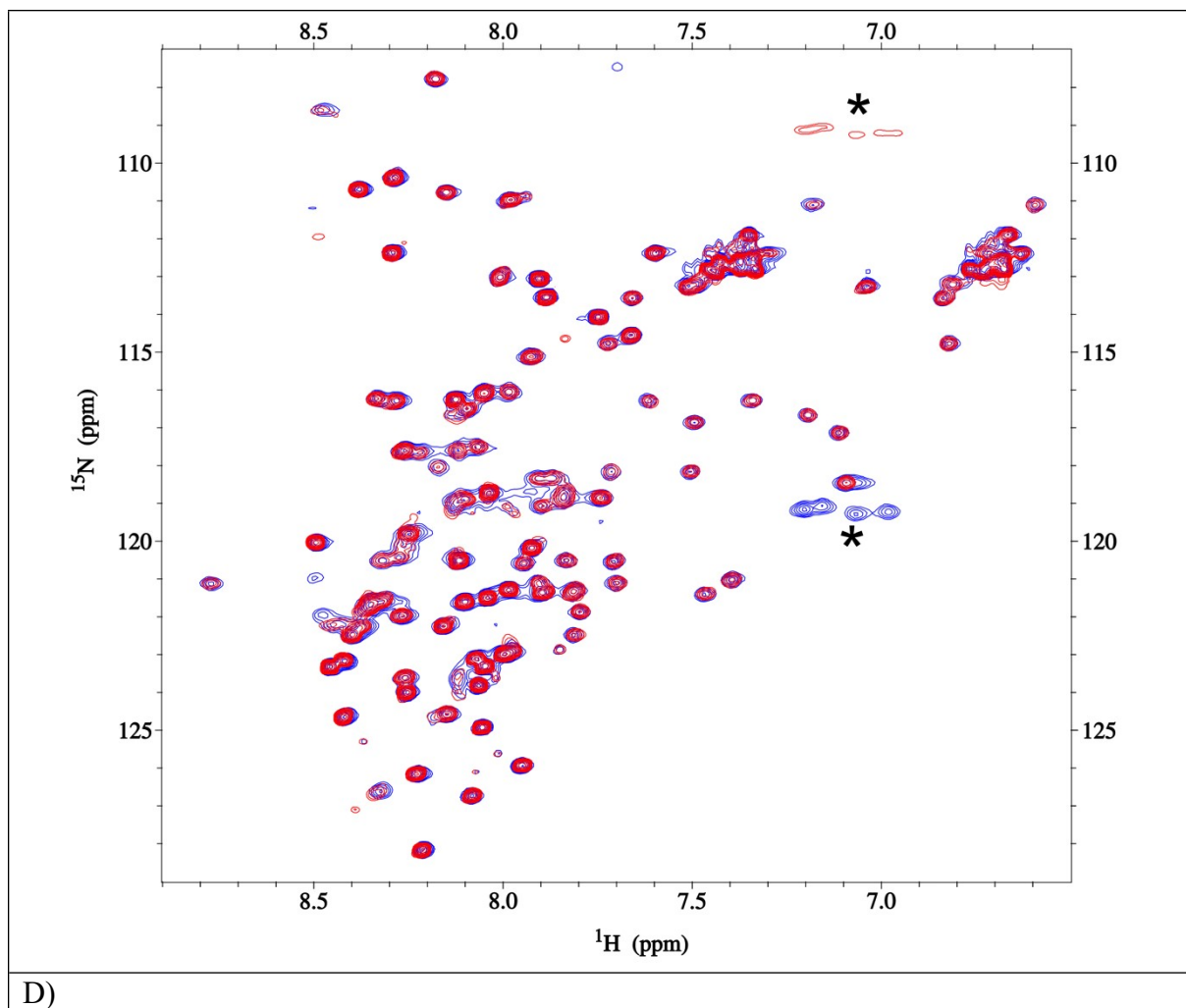
A)



B)



C)



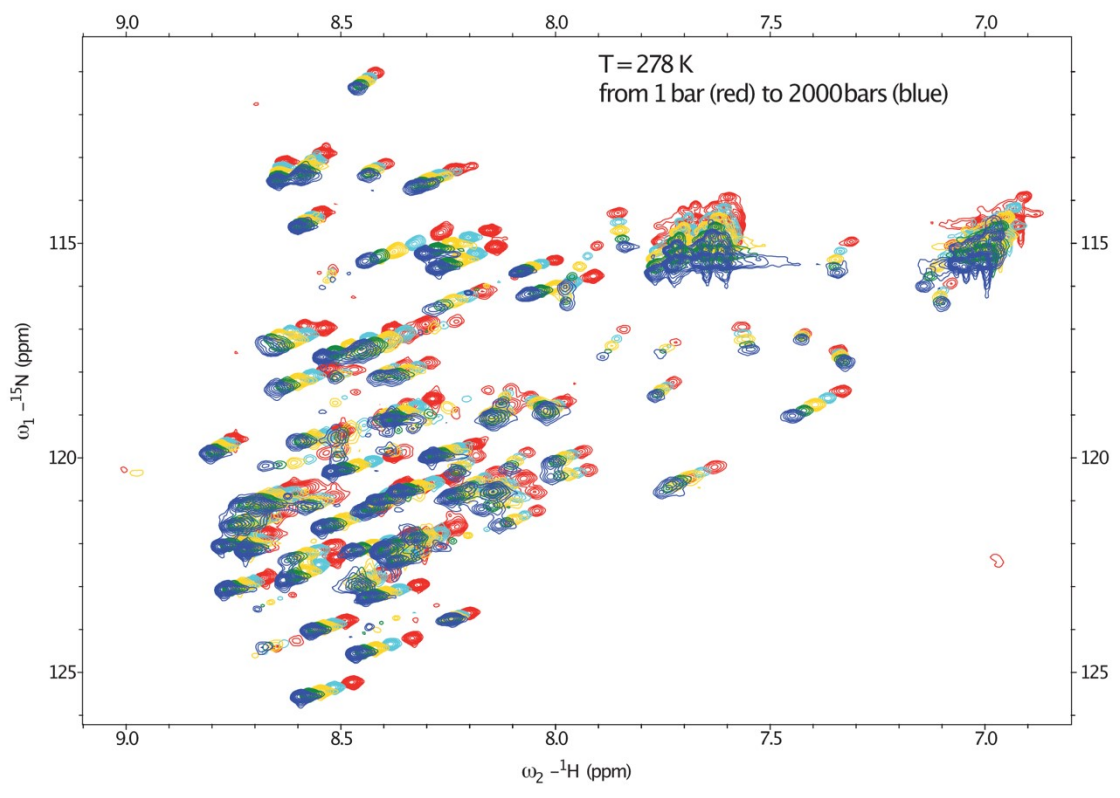
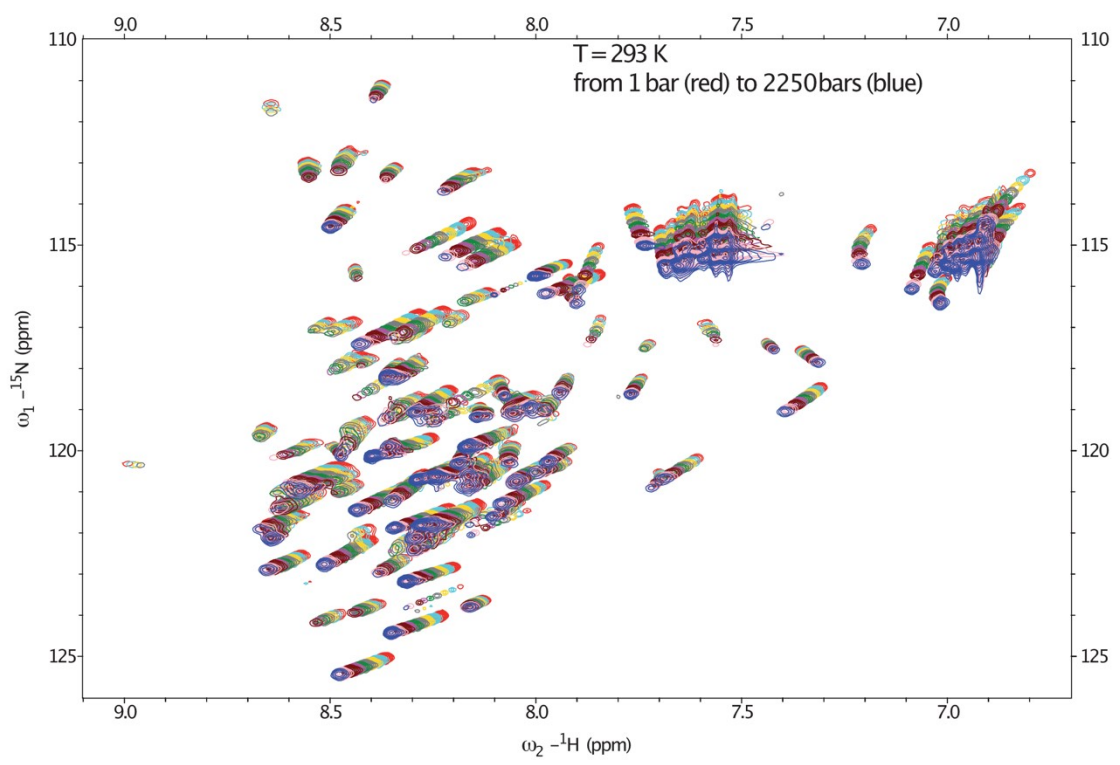
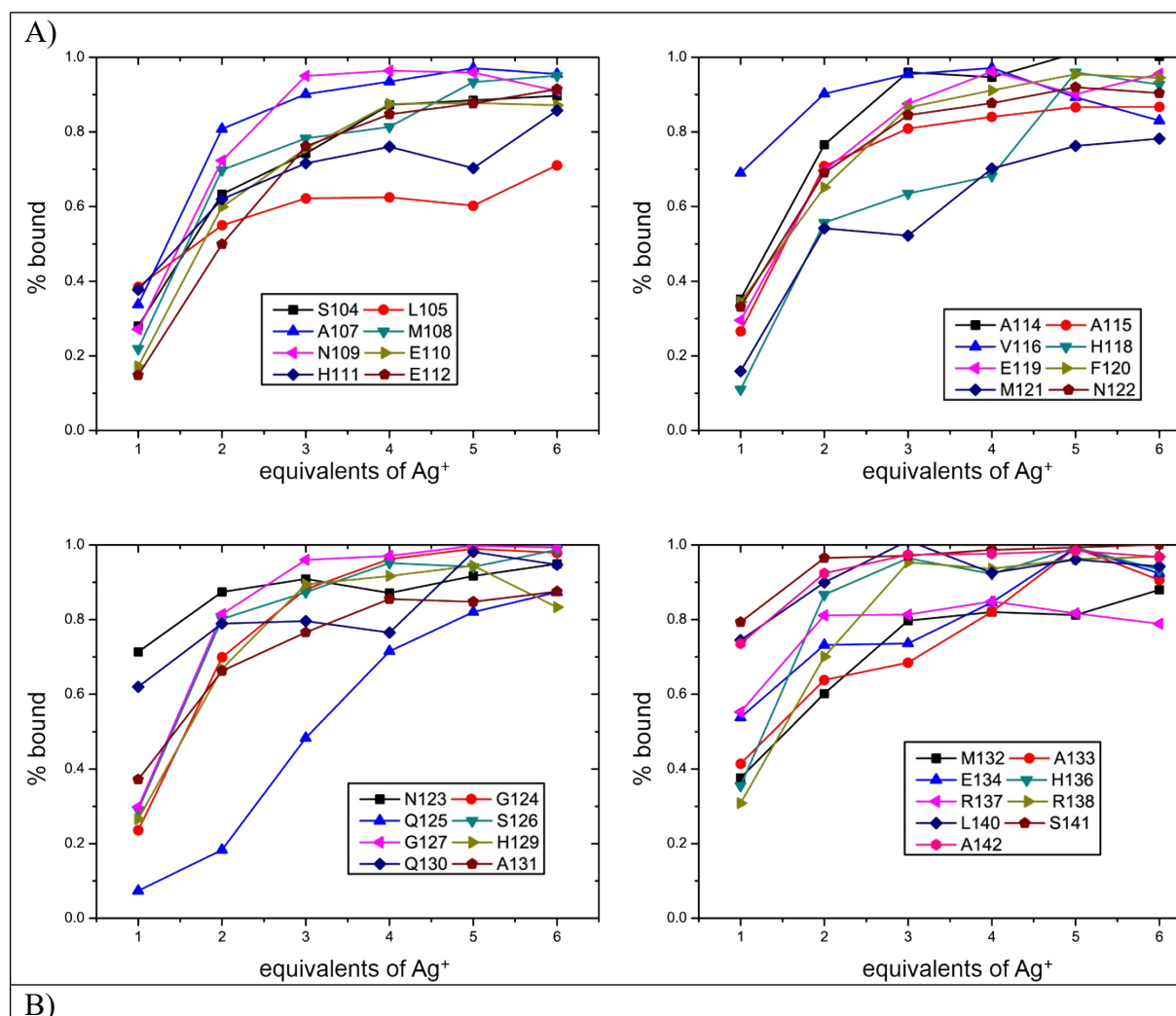


Fig. S5 | A) Proportion of bound state as a function of Ag^+ equivalent calculated from the NMR signal ratio between free and bound state for residues 104 to 142. B) Evolution of signal intensity for residues affected by slow to intermediate exchange.



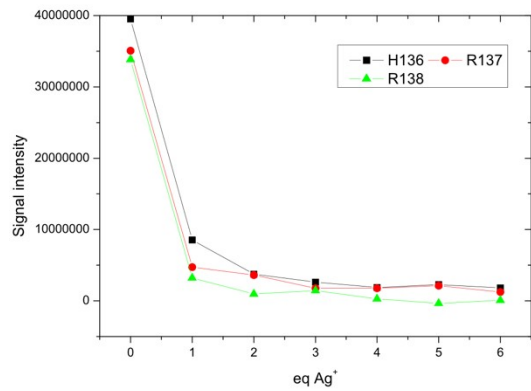
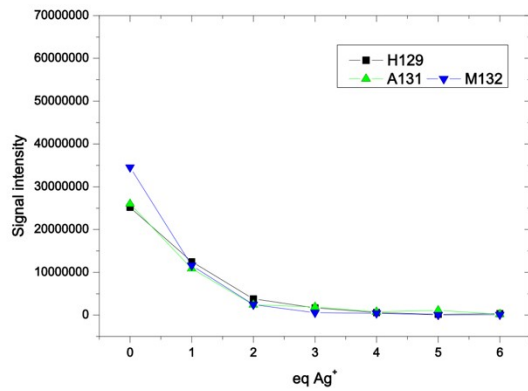
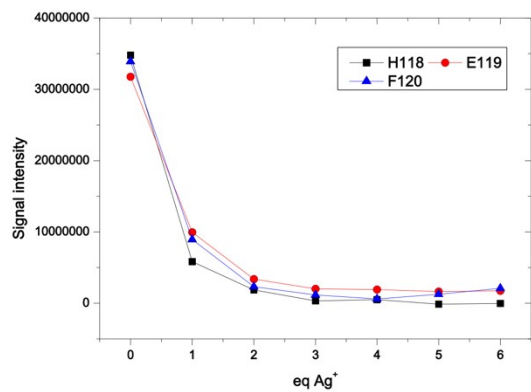
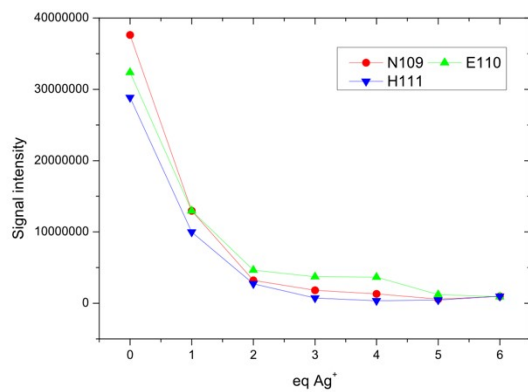
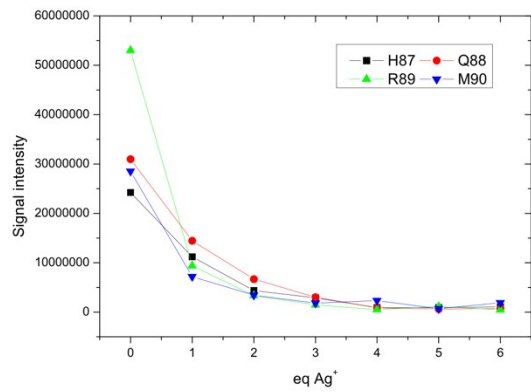
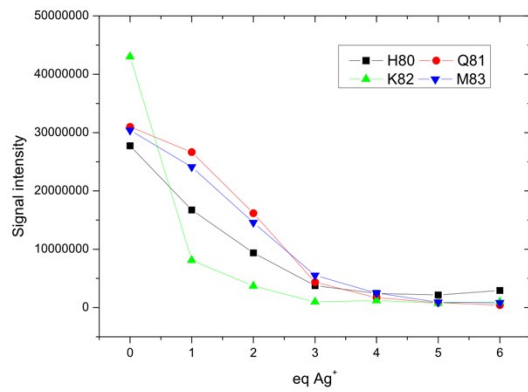
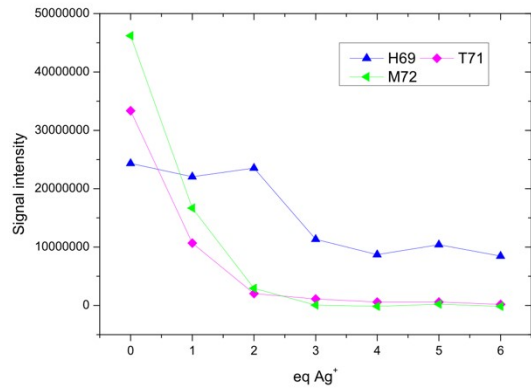
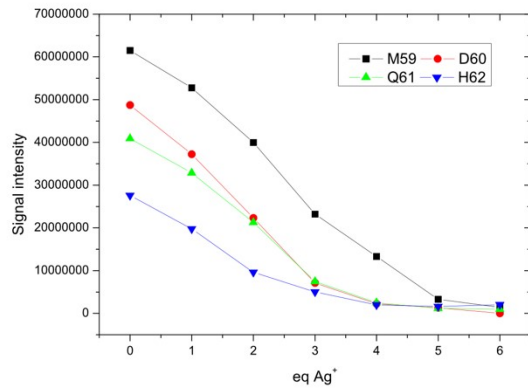


Fig. S6 | CD curves recorded at 25°C for free SiIE⁵⁷⁻⁹⁵ and in presence of 1 to 6 equivalents of silver ions and ([SiIE⁵⁷⁻⁹⁵] = 20 μM in 20 mM MES buffer pH 6.8 implemented with 20 mM NaF). Ten repetitions have been recorded for each sample.

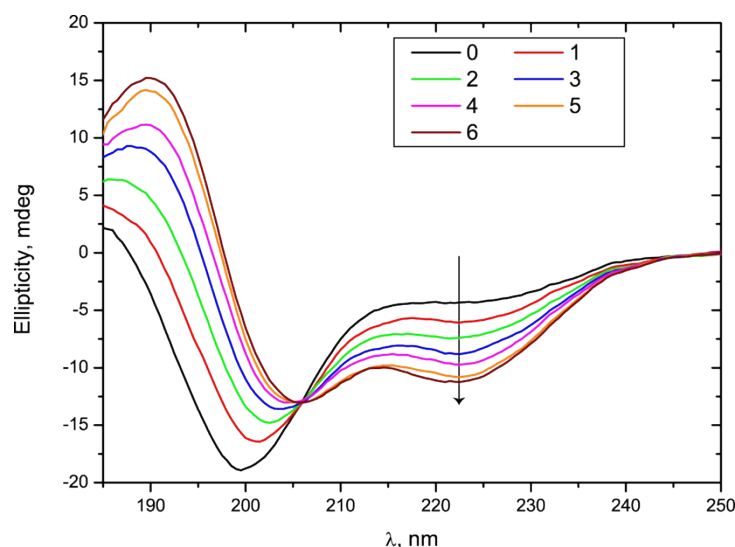


Fig. S7 | SAXS data curve for A) free SiIE and B) SiIE + 6 equivalents Ag⁺ in solution.

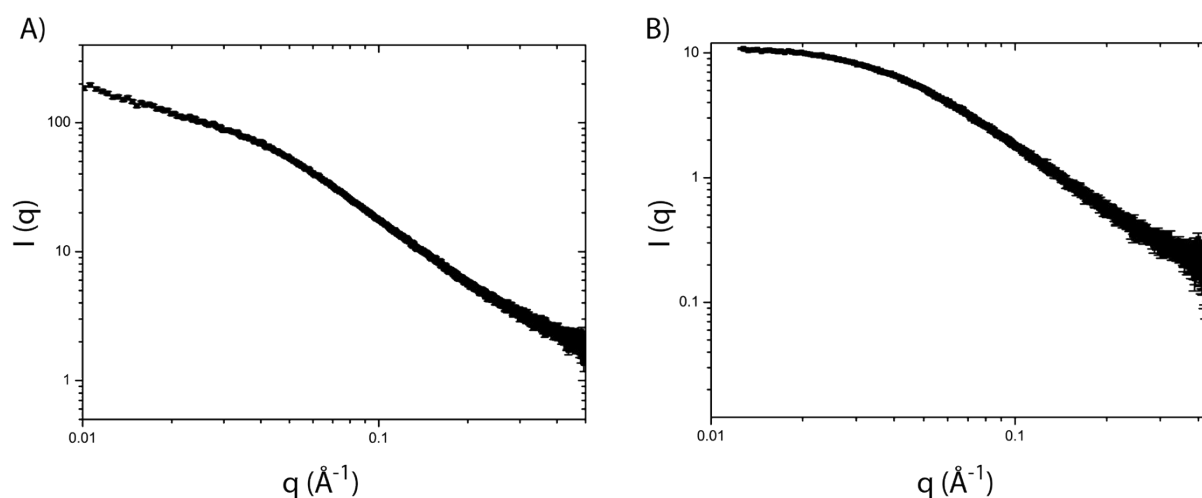


Fig. S8 | Overlay of the modeled structures of SiIE using AlphaFold with two possible arrangements A) rank1 in globular form and B) rank2 elongated form and the different NMR structures of the SiIE mimicking peptides. The respective peptides have been colored according to their structure with the following: structures A1 (magenta), A2 (pink), B1 (yellow), and B2 (blue). Noteworthy is the remarkable agreement between the individual peptide structures and the AlphaFold predicted α -helical structures.

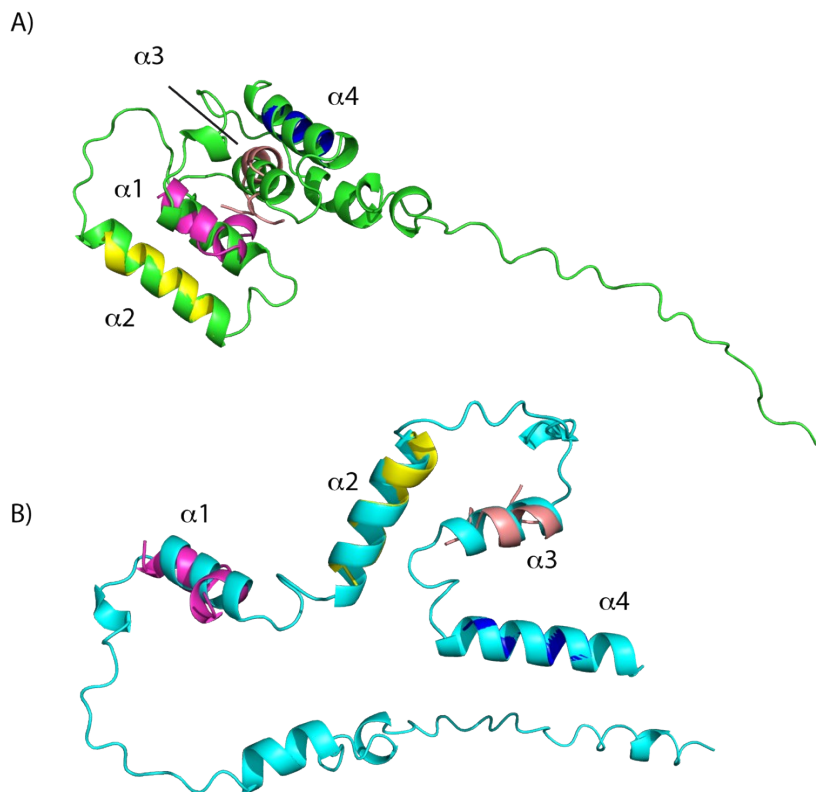


Fig. S9 | Detailed analysis of AlphaFold results and models prediction accuracy. (A) The pLDDT (predicted IDDT-C α) is shown alongside the Ag-SilE secondary structure (top) without the signal peptide sequence 'MKNIVLASLLGFGLISSAWA'. The different models express high confidence in the different structured helical regions α_1 , α_2 , α_3 , and α_4 while the remaining regions may be unstructured in isolation (see methods). (B) The different heat maps show the Predicted Aligned Errors (PAE) that estimate the confidence about the domain's positioning. A PAE below 5 Å indicates that AlphaFold is confident about domain positioning. (C) AlphaFold modeled structures showing their diversity in terms of structural sampling and colored according to the pLDDT from red (low pLDDT) to blue (high pLDDT).

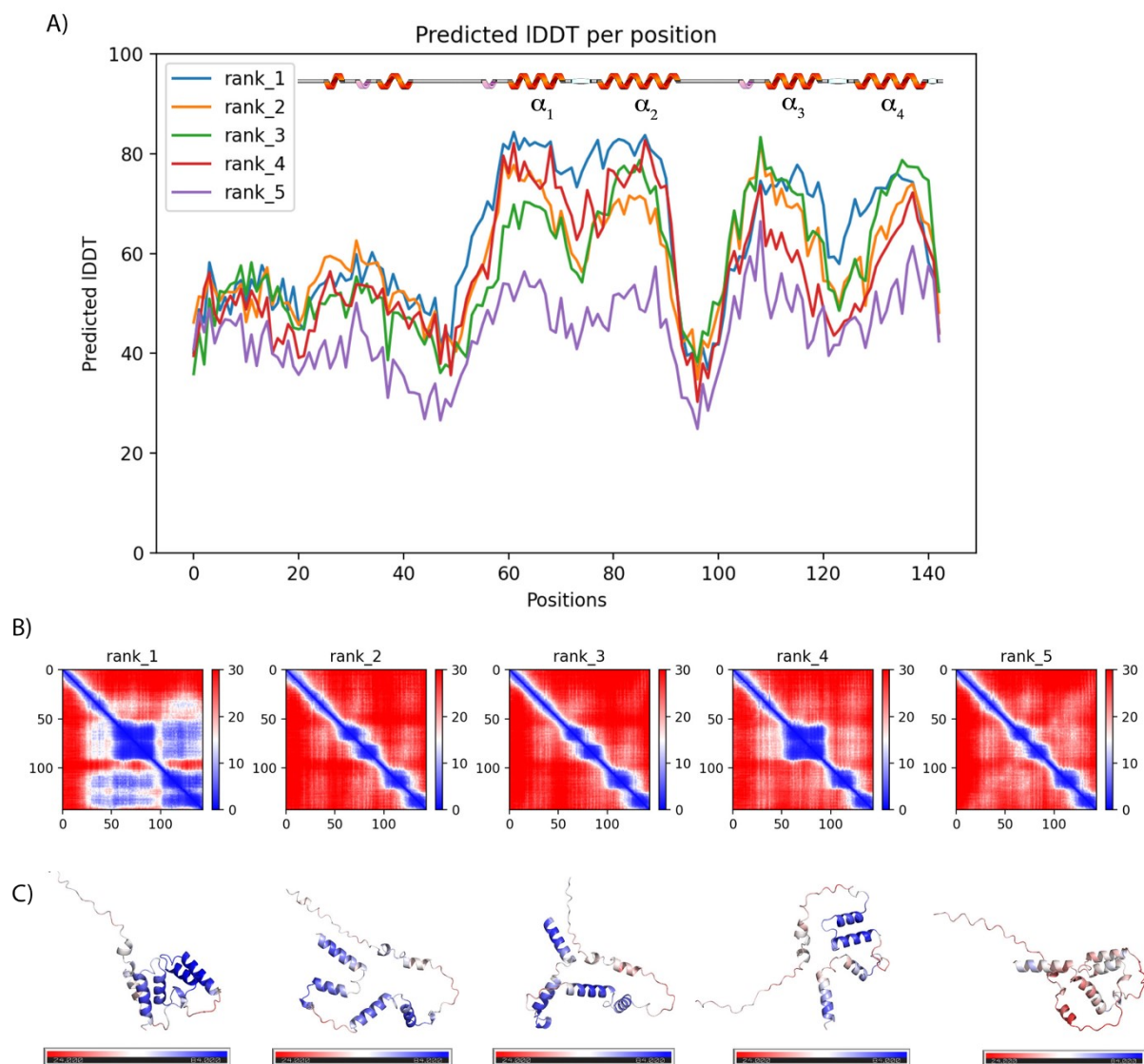


Fig. S10 | Dependence of the relaxation rates R_1 , R_2 and hetNOE on the microdynamic parameters according to the Lipari & Szabo model in the case of axial anisotropy (analytical expression can be found in Chen et al., *J Chem Theory Comput*, **2018**, 14 (2), 1009-1019). Relaxation data have been calculated for three different orientations of an NH vector (left panel) with respect to the principal axis system (green). The data shown here were calculated for a correlation time $\tau_c = 5$ ns, assuming the NMR frequency of 600 MHz and a moderate anisotropy of 1.4. Black dots represent the relaxation parameters for different order parameter values and local motion (S^2, τ_{loc}). The respective values for S^2 are: 0.2, 0.4, 0.6 and 0.9 along with 2.0, 1.0, 0.4 and 0.1 ns for the local motion. It is noticeable that a decrease of τ_{loc} and an increase of S^2

induces a slight decrease of R_1 and a significant increase of R_2 and hetNOE and confirm the structural rigidification seen in our study.

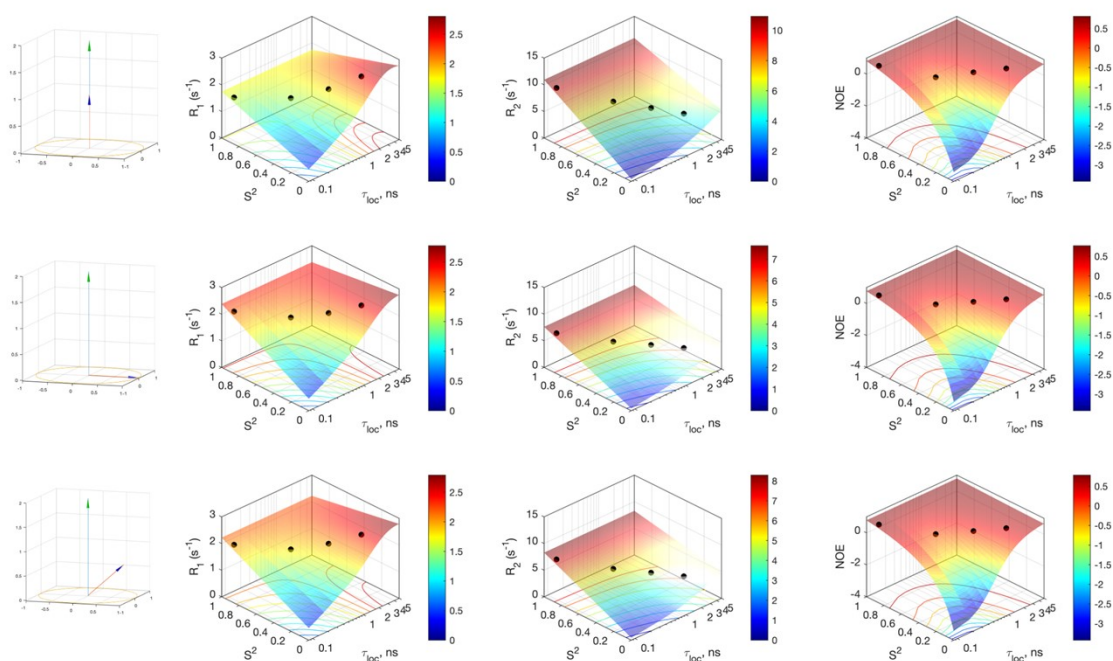
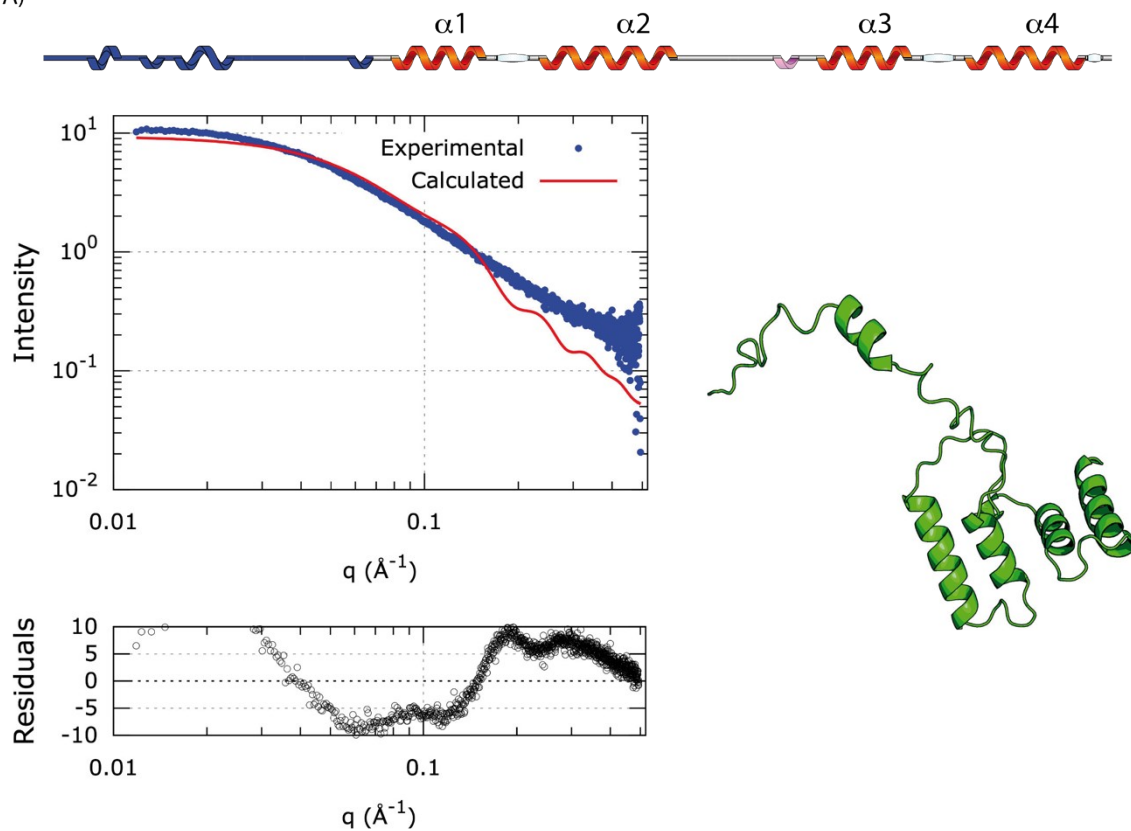


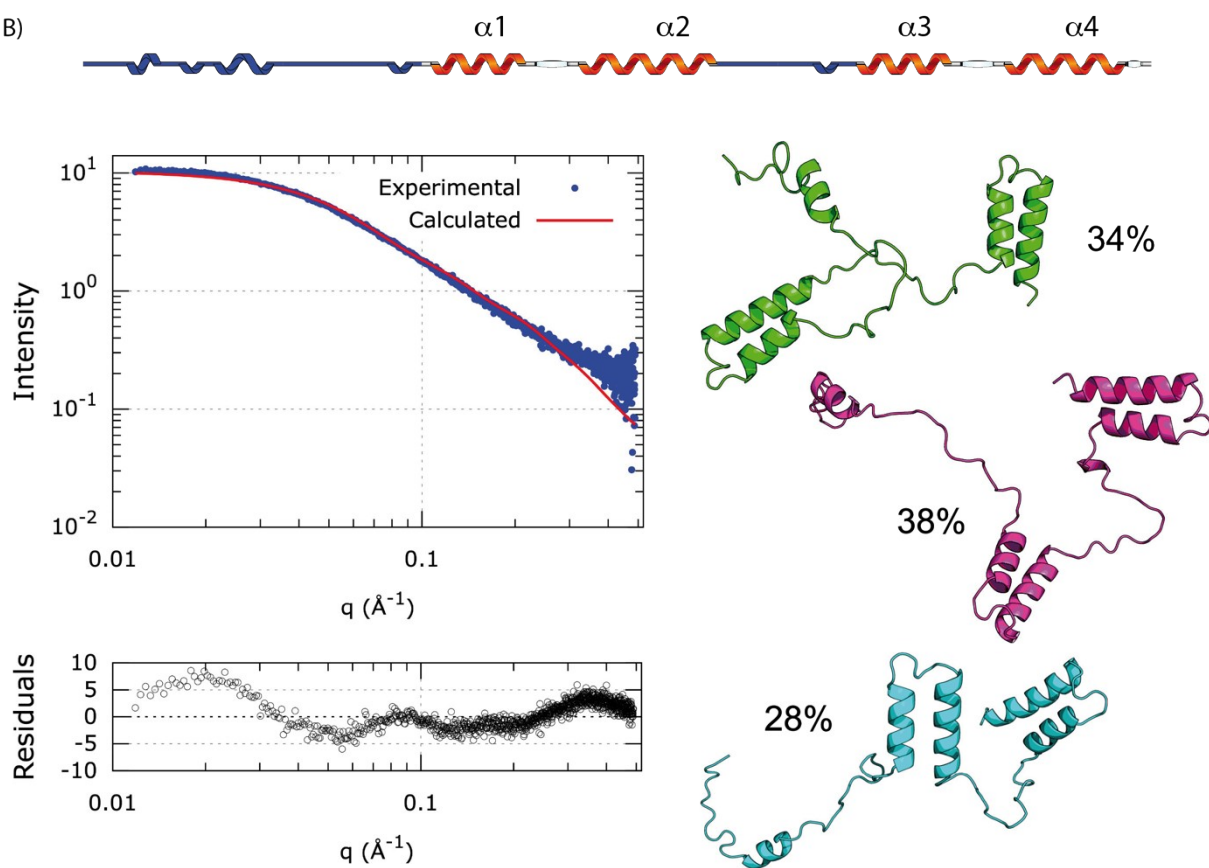
Fig. S11 | SAXS analysis of Ag-SilE complex. On top, the [SilE:nAg] complex secondary structure deduced from AlphaFold is sketched. The different flexible segments used in the MultiFoXS calculation are colored in blue. SAXS data (blue circle), back-calculated SAXS data (red line), and residuals are represented on the left panel. On the right panel, the representation of the top-scoring N-ensemble of structures and their respective weight that best fit the SAXS data is presented close to each structure and are determined using the MultiFoXS server. Residuals per i^{th} SAXS data point have been calculated according to the following expression: $(I(q_i)^{\text{exp}} - I(q_i)^{\text{calc}}) / \sigma_i$. $I(q_i)^{\text{exp}}$ is the measured scattering intensity, $I(q_i)^{\text{calc}}$ is the intensity calculated using MultiFoXS for scattering vector q_i and σ_i is the experimental error.

In panel A) the rank1 compact structure (only the N-terminus is flexible), B) the linker between α_2 and α_3 is flexible, C) the linkers between α_1 / α_2 and α_2 / α_3 are flexible, and D) the linkers between α_2 / α_3 and α_3 / α_4 are flexible.

A)



B)



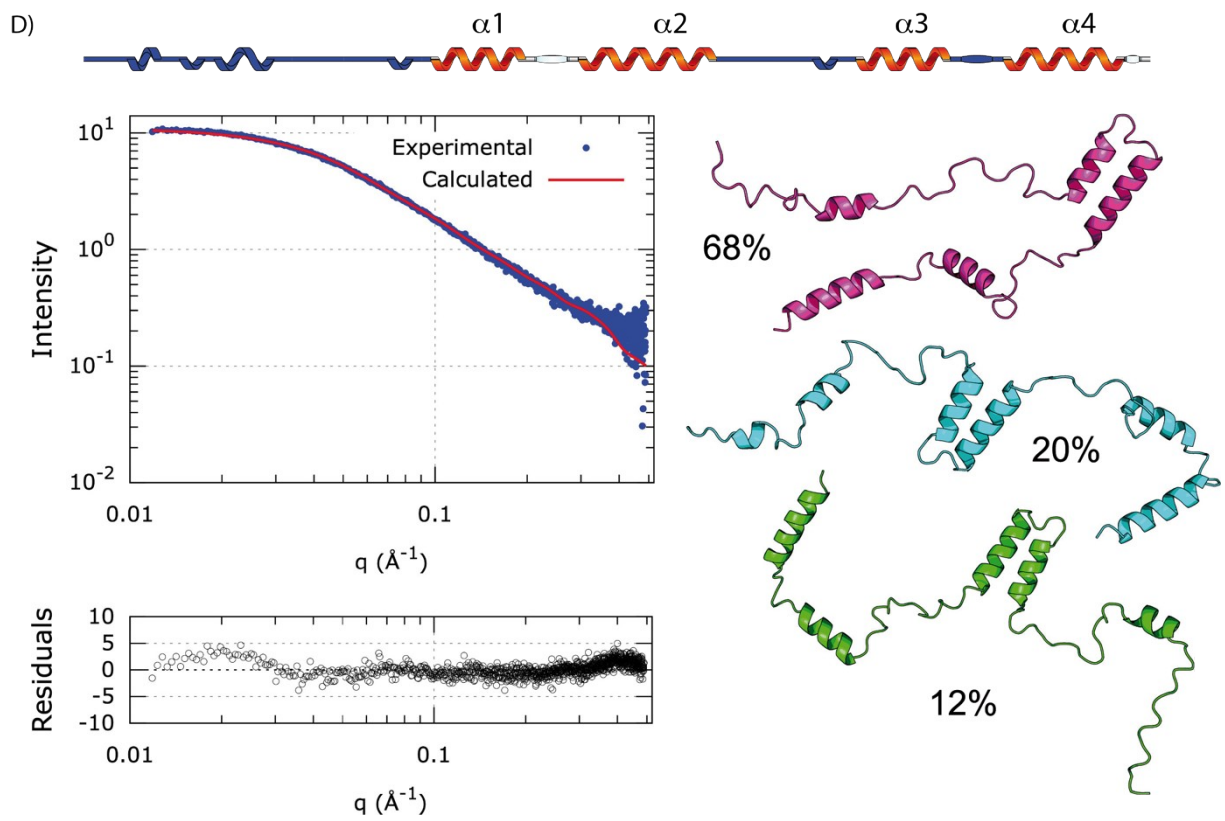
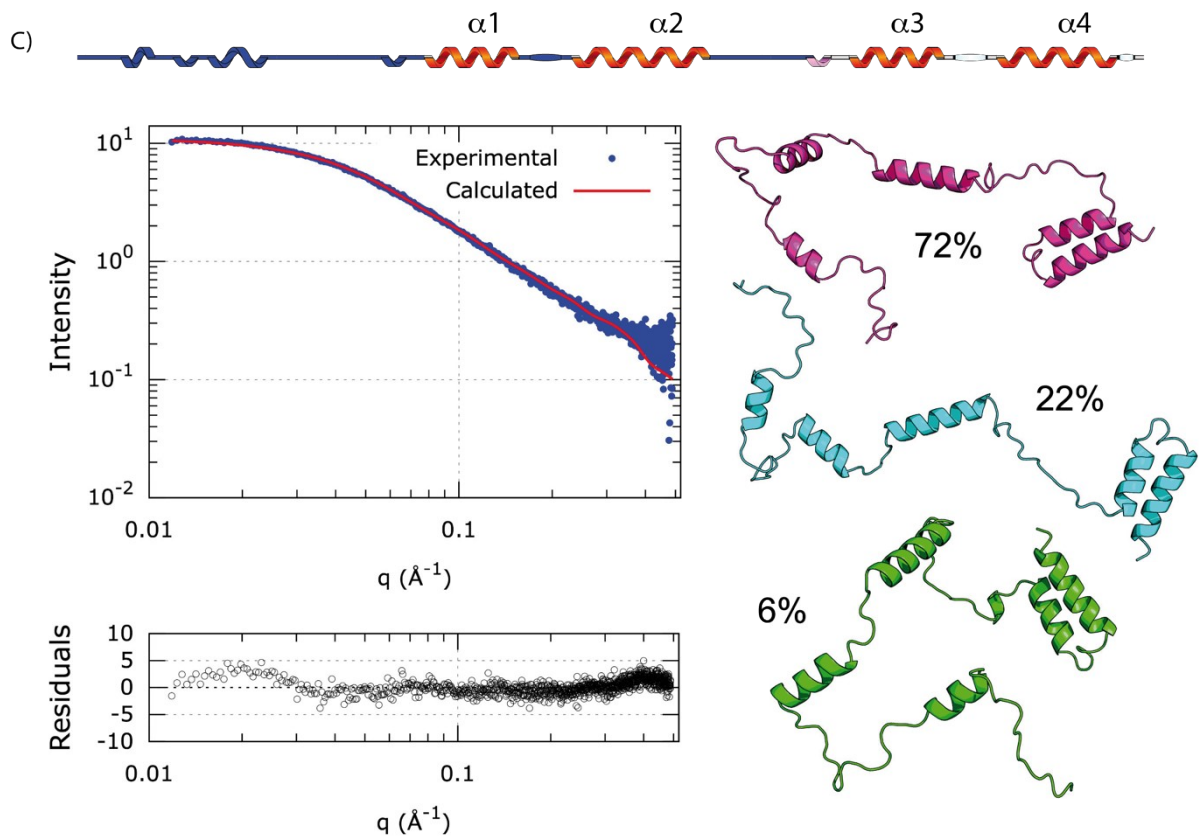


Table S1 | List of protonated peptides identified by LC-MS/MS after digestion of SiIE A) and SiIE + 6 equivalents of silver ions B).

A) Peptide	PTMs	Score	<i>m/z</i>	ppm	Charge
VNNAQAPAHQMQSAAAPVGIQGTAPR		93.3	1293.14785	-4.6	2
AAVAHEFMNNGQSGPHQAMAEHR	Oxidation (M8)	59.5	645.039143	-4.6	4
VNNAQAPAHQMQSAAAPVGIQGTAPR	Oxidation (M11)	55.4	867.766638	-3.7	3
MAGMDQHEQAIIAHETMTNGSADAHQK	Oxidation (M1); Oxidation (M17); Asn->Asp (N19)	54.5	985.757979	-2.4	3
MMGSQTVSPTGPSK	Oxidation (M2)	48.6	712.329005	-3.4	2
MMGSQTVSPTGPSK	Oxidation (M1)	48.6	712.329005	-3.4	2
MMGSQTVSPTGPSK	Oxidation (M1); Oxidation (M2)	46.2	720.327332	-2.1	2
MMGSQTVSPTGPSK		46.1	704.331463	-3.5	2
SLAAMNEHER	Oxidation (M5)	46	587.267711	-2.9	2
SLAAMNEHER		42.2	579.269306	-4.7	2

B) Peptide	PTMs	Score	<i>m/z</i>	Ppm	Charge
MAGMDQHEQAIIAHETMTNGSADAHQK	Asn->Asp (N19)	69	975.0933	-3.8	3
VNNAQAPAHQMQSAAAPVGIQGTAPR	Oxidation (M11)	67.3	1301.142	-6.9	2
VNNAQAPAHQMQSAAAPVGIQGTAPR		63.5	862.4306	-8.9	3
MMGSQTVSPTGPSK	Oxidation (M2)	48.7	712.3288	-3.6	2
MMGSQTVSPTGPSK	Oxidation (M1)	48.7	712.3288	-3.6	2
MMGSQTVSPTGPSK		46.1	704.3285	-7.8	2
MMGSQTVSPTGPSK	Oxidation (M1); Oxidation (M2)	46.1	720.3245	-6.1	2
SLAAMNEHER		42.1	579.2673	-8.1	2
SLAAMNEHER	Oxidation (M5)	20.3	391.8454	-8.5	3

Table S2 | Summary of the lowest χ scores for SiIE depending on the number of flexible regions (sketched in blue) and for the different N-state models used in MultiFoXS after the computation of 1000 conformations and starting from 10000 initial conformations. The highest χ scores for the top 1000 models are given in parentheses. The white part is maintained as rigid during calculation. Except for the first case, the 3-states models have been chosen to describe the conformational sampling of SiIE in the different cases (χ scores colored in red). Average radii of gyration and standard deviation of each chosen N-states model are also given in the last column.






	χ					Rg (Å)
	1 state	2 states	3 states	4 states	5 states	
	37.4 (146.8)	N.A	N.A	N.A	N.A	24.6
	7.3 (158.8)	6.6 (8.8)	6.3 (6.8)	6.2 (6.4)	6.2 (6.2)	33.9 (1.8)
	2.55 (22.9)	2.0 (3.0)	1.9 (2.0)	1.9 (1.9)	1.9 (1.9)	28.9 (1.4)
	2.3 (38.2)	1.9 (2.3)	1.9 (1.9)	1.9 (1.9)	N.A	31.9 (4.0)
	1.8 (15.9)	1.0 (1.6)	0.9 (1.0)	0.9 (0.9)	0.9 (0.9)	33.6 (3.7)

Table S3 | Solvent accessibility surface area (SASA) calculated for HIS and MET residues involved in silver binding for the globular structure (Fig. S10A) and the different structures determined when SilE is fully flexible (Fig. 6). The weighting average value is calculated according to the different weights associated with each structure of Fig. 6.

Residues	Globular structure	Fully flexible structure		
		Structure 1	Structure 2	Structure 3
MET 59	53	47.3	47.6	54.1
HIS62	25.7	82.7	93.4	82.6
HIS69	24.6	76	57.7	72.5
MET72	59.1	91	83 .1	69.8
HIS80	23.9	67.1	52.6	74.9
MET83	56.6	72.3	72.3	72.3
HIS87	17.7	68.3	68.3	68.3
MET90	59.6	77.1	72.7	72.5
MET108	10.5	71.4	47.5	62.8
HIS111	44.5	97.5	94.3	100
HIS118	21.8	72.5	70.3	71.2
MET121	44.8	74	71.4	74
HIS129	25.7	46.7	37.1	59.9
MET132	51.1	67.4	64.8	67.4
HIS136	24.1	74.4	74.4	74.4
MET139	52.7	69.8	69.8	69.8
Average value	37.2	72.2	67.3	71.7
Weighting average value			70.2	

References

1. T. N. S. Huynh, D. Bourgeois, C. Basset, C. Vidaud and A. Hagege, *Electrophoresis*, 2015, **36**, 1374-1382.
2. H. Barsnes and M. Vaudel, *Journal of Proteome Research*, 2018, **17**, 2552-2555.
3. D. Bouyssie, A. M. Hesse, E. Mouton-Barbosa, M. Rompais, C. Macron, C. Carapito, A. G. de Peredo, Y. Coute, V. Dupierris, A. Burel, J. P. Menetrey, A. Kalaitzakis, J. Poisat, A. Romdhani, O. Burlet-Schiltz, S. Cianferani, J. Garin and C. Bruley, *Bioinformatics*, 2020, **36**, 3148-3155.
4. A. L. Simon, F. Chiro, C. M. Choi, C. Clavier, M. Barbaire, J. Maurelli, X. Dagany, L. MacAleese and P. Dugourd, *The Review of scientific instruments*, 2015, **86**, 094101.
5. P. Pernot, A. Round, R. Barrett, A. De Maria Antolinos, A. Gobbo, E. Gordon, J. Huet, J. Kieffer, M. Lentini, M. Mattenet, C. Morawe, C. Mueller-Dieckmann, S. Ohlsson, W. Schmid, J. Surr, P. Theveneau, L. Zerrad and S. McSweeney, *Journal of synchrotron radiation*, 2013, **20**, 660-664.
6. P. V. Konarev, V. V. Volkov, A. V. Sokolova, M. H. J. Koch and D. I. Svergun, *Journal of Applied Crystallography*, 2003, **36**, 1277-1282.

7. S. Förster, L. Apostol and W. Bras, *Journal of Applied Crystallography*, 2010, **43**, 639-646.
8. M. Mirdita, K. Schütze, Y. Moriwaki, L. Heo, S. Ovchinnikov and M. Steinegger, *Nature Methods*, 2022, **19**, 679-682.
9. J. Jumper, R. Evans, A. Pritzel, T. Green, M. Figurnov, O. Ronneberger, K. Tunyasuvunakool, R. Bates, A. Žídek, A. Potapenko, A. Bridgland, C. Meyer, S. A. A. Kohl, A. J. Ballard, A. Cowie, B. Romera-Paredes, S. Nikolov, R. Jain, J. Adler, T. Back, S. Petersen, D. Reiman, E. Clancy, M. Zielinski, M. Steinegger, M. Pacholska, T. Berghammer, S. Bodenstein, D. Silver, O. Vinyals, A. W. Senior, K. Kavukcuoglu, P. Kohli and D. Hassabis, *Nature*, 2021, **596**, 583-589.
10. V. Mariani, M. Biasini, A. Barbato and T. Schwede, *Bioinformatics*, 2013, **29**, 2722-2728.
11. K. Tunyasuvunakool, J. Adler, Z. Wu, T. Green, M. Zielinski, A. Žídek, A. Bridgland, A. Cowie, C. Meyer, A. Laydon, S. Velankar, G. J. Kleywegt, A. Bateman, R. Evans, A. Pritzel, M. Figurnov, O. Ronneberger, R. Bates, S. A. A. Kohl, A. Potapenko, A. J. Ballard, B. Romera-Paredes, S. Nikolov, R. Jain, E. Clancy, D. Reiman, S. Petersen, A. W. Senior, K. Kavukcuoglu, E. Birney, P. Kohli, J. Jumper and D. Hassabis, *Nature*, 2021, **596**, 590-596.
12. D. Schneidman-Duhovny, M. Hammel, J. A. Tainer and A. Sali, *Nucleic Acids Research*, 2016, **44**, W424-W429.